Multiple phase transitions and the effect of disorder in the locally noncentrosymmetric ferromagnet $URhGe_2$

Daniel Gnida,* Maria Szlawska, and Marek Daszkiewicz
Institute of Low Temperature and Structure Research, Polish Academy of Sciences, ulica Okólna 2, 50-422 Wrocław, Poland

(Received 4 April 2023; revised 3 September 2023; accepted 7 December 2023; published 29 December 2023)

The locally noncentrosymmetric ferromagnet $URhGe_2$, which undergoes ordering at the Curie temperature $T_C = 25$ K, was subjected to a comprehensive investigation employing x-ray diffraction, magnetic susceptibility, electrical resistivity, and specific heat measurements. Our results reveal a significant heat capacity anomaly in the paramagnetic state near 30 K which is due to two simultaneous phase transitions characterized by temperatures $T_s \simeq 29.5$ K and $T_m \simeq 30$ K. In particular, with increasing applied magnetic field, T_m shifts to higher temperatures, while T_s remains unaffected, suggesting a different nature of these transitions and leading to a complex temperature-magnetic field phase diagram. The field-independent phase transition can be interpreted in terms of structural distortions, while the second transition defies typical behavior for ferro- or antiferromagnetic phases, suggesting a more intricate magnetic structure or multipole ordering. The electron transport shows strong anisotropy, not only in the magnitude of the resistivity but also in its temperature dependence. The three times higher residual resistivity along the crystallographic c axis, compared to the a axis component significantly influences its temperature dependence. While the a-axis resistivity behaves typically for normal ferromagnets, the c-axis resistivity shows a minimum in its temperature dependence well below T_C. This behavior results from the competition between electron spin wave scattering and quantum corrections, dominated by the $A_{QC}T^{1/2}$ contribution due to impurity scattering assisted electron-electron interaction. Remarkably, the $A_{QC}T^{1/2}$ dependence with a comparable A_{QC} coefficient is also observed for $T \gg T_C$, indicating the relevance of interaction quantum effects in electron transport also in the paramagnetic state.

DOI: 10.1103/PhysRevB.108.235174

I. INTRODUCTION

Recently, there has been a growing focus on locally noncentrosymmetric electron systems within the field of condensed matter physics. Research has shown that, even when the global inversion symmetry of a crystal remains intact, specific instances of local symmetry violation can lead to the emergence of novel exotic phases. These locally noncentrosymmetric structures are commonly studied in layered crystals [1], as well as in artificial superlattices [2,3] and crystals exhibiting structural disorder [4–7]. Recently, particular attention has been directed towards understanding the physics of local symmetry breaking, with a special focus on its connection to superconductivity [1,8–11]. Theoretical predictions suggest that certain features associated with noncentrosymmetric superconductors, such as parity mixing of Cooper pair states and their unconventional response to magnetic fields, may also manifest in electron systems in which inversion symmetry is only locally broken. It is important to note, however, that local noncentrosymmetry can also give rise to a variety of other emergent properties, including odd-parity multipole ordering [12–14], the formation of complex magnetic textures [15,16], and even the development of boson peaks in glasses or defective crystals [6].

Among numerous electronic systems, a considerable number of representatives of f-electron compounds with locally broken inversion symmetry exist [1,12]. Interestingly, the ferromagnetic superconductors UGe_2 [17], URhGe [18], and UCoGe [19] also fall into this category of multiorbital systems. In these compounds, uranium atoms form three-dimensional coupled zigzag chains, representing a characteristic example of crystal structures lacking local inversion symmetry. This particular structural motif is believed to play a role in promoting unconventional superconductivity [20], as well as being discussed in the context of odd-parity multipole ordering due to local parity mixing [12,13]. The peculiar properties exhibited by this group of compounds thus motivate the search for new locally noncentrosymmetric uranium germanides or a more comprehensive investigation of existing ones.

In recent years, nonstoichiometric ternary germanides with the general formula $UT_{1-x}Ge_2$, where T represents a transition-metal element, have garnered significant attention due to their close structural resemblance to the orthorhombic $ZrGa_2$ crystal structure adopted by UGe_2. Previous investigations categorized these compounds into two distinct groups based on their crystal symmetry. In particular, iron- and nickel-based compounds crystallize in the orthorhombic $CeNiSi_2$-type structure, while those containing ruthenium or osmium exhibit a monoclinic phase with a novel structure [21–26]. Notably, $UFe_{0.39}Ge_2$, $URu_{0.29}Ge_2$, and $UOs_{0.25}Ge_2$ exhibit ferromagnetic behavior with Curie temperatures T_C of 37 K [21], 63 K [24], and 54 K [26], respectively. In contrast, $UNi_{0.45}Ge_2$ has been reported to display antiferromagnetic ordering with a Néel temperature T_N

*d.gnida@intibs.pl

 ©2023 American Physical Society

of 47 K [22,23]. Importantly, these studies have revealed that irrespective of the magnetic ground state, structural disorder strongly influences electron conduction in these compounds, leading to the emergence of quantum interference effects in the electrical resistivity well below the magnetic phase transition [21,22,24].

Among the compounds with the general formula $UT_{1-x}Ge_2$, one can also distinguish those with $x = 0$. In contrast to their transition-metal-deficient counterparts, the stoichiometric variants adopt a $YIrGe_2$-type crystal structure. It is important to emphasize that, as in the nonstoichiometric compounds, none of the atoms occupy special positions in the unit cell where an inversion center exists. Consequently, the coordination environment of each atom in the centrosymmetric crystal structure is noncentrosymmetric. However, despite the existence of numerous locally noncentrosymmetric phases of $YIrGe_2$ [27], only two uranium-based compounds, $UIrGe_2$ [28] and $URhGe_2$ [28,29], have been reported. $UIrGe_2$ exhibits simple paramagnetic behavior with no observed phase transitions, whereas $URhGe_2$ shows ferromagnetic properties with $T_C = 25$ K and the easy axis of magnetization oriented along the longest lattice constant [29]. Interestingly, $URhGe_2$ undergoes an additional phase transition at 30 K, manifested only in electrical resistivity and heat capacity measurements, with no clear indication in magnetic susceptibility [29]. Furthermore, resistivity measurements indicate that the temperature of this phase transition increases under external pressure [30], although the origin of this transition remains a mystery.

Consequently, we carried out further investigations of single crystalline $URhGe_2$ to gain a deeper understanding of the underlying nature of the phase transitions observed in the paramagnetic state. Our study focused on exploring the magnetic field dependence of the physical properties of $URhGe_2$, which allowed us to construct an H-T phase diagram. In addition, we present a comprehensive analysis of the electron transport properties of $URhGe_2$ probed by electric current along two different crystallographic directions, termed a and c. Our results show that distinctly different temperature dependences of the resistivities, ρ_a and ρ_c, arise from their respective residual values, which are strongly anisotropic in the studied $URhGe_2$.

II. EXPERIMENTAL DETAILS

A single crystal of $URhGe_2$ was grown in an ultrapure argon atmosphere with the Czochralski pulling technique using a tetra-arc furnace. X-ray diffraction data were collected on an Oxford Diffraction four-circle single-crystal diffractometer. Raw data were processed using the CRYSALIS data reduction program (CRYSALISPRO version 1.171.42.49). Absorption correction was applied to optimize the crystal size and shape. The computer programs SHELXS-2018, SHELXL-2018, and SHELXLE [31–33] were used, along with DIAMOND version 3.2k for visualization [34]. The magnetic properties of the compound were measured in the temperature range 1.72–400 K and in magnetic fields up to 7 T using a Quantum Design MPMS-7 superconducting quantum interference design magnetometer. Heat capacity was measured over the temperature range of 2–60 K and in magnetic fields up to 9 T using a Quantum Design PPMS-9 platform. Four-point AC resistivity was measured in magnetic fields up to 9 T using a Quantum Design PPMS-9 device in the temperature range of 2–300 K. Resistivity measurements were made on oriented single-crystalline samples with current flowing along the a and c axes of the crystallographic unit cell.

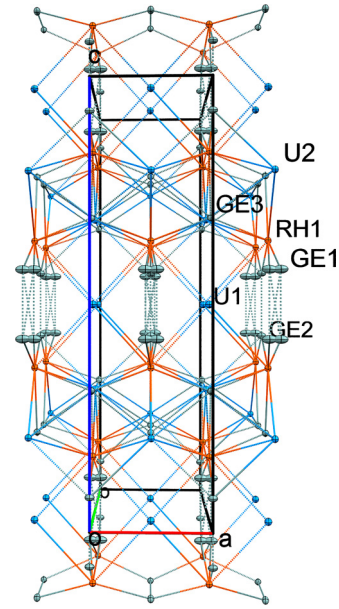

FIG. 1. Perspective view of the crystal packing of $URhGe_2$.

III. RESULTS AND DISCUSSION

A. Crystal structure and thermodynamic properties

A perspective view of the crystal packing and unit cell of $URhGe_2$ is shown in Fig. 1, while crystal data and structure refinement details for $URhGe_2$ are presented in Table I. The x-ray diffraction measurements confirm that $URhGe_2$ crystallizes in the orthorhombic crystal system (space group $Immm$) and adopts the structure type of $YIrGe_2$ [35]. The obtained lattice parameters are in good agreement with the previously reported data [28,35]. All the atoms are placed in special positions, i.e., U1 in the $m2m$ site symmetry and 4h Wyckoff position, U2 in $m2m$ and 4j, Rh1 in $m..$ and 8l, Ge1 in $.m.$ and 8m, Ge2 in $mm2$ and 4i, and Ge3 in $m..$ and 8l. The atomic coordinates and displacement parameters are given in Tables II and III, respectively. In the preliminary stages of the crystal structure refinement, a large value of the parameter U_{11} was observed for the Ge1 atom. This structural model is very similar to the recently reported high-temperature phase of $YPtGe_2$ and $GdPtGe_2$ [27], but the prolate ellipsoid for Ge1 in $URhGe_2$ is more pronounced, and therefore, the Ge1 atom is split into two positions in the final model. Since these two positions are related to each other by the mirror plane perpendicular to the a axis at a relatively short distance of 0.392(15) Å, the site occupancy factor was set to 0.5. Thus, the splitting describes a disorder of the Ge1 atom along the a direction, and no additional germanium atoms were included in the definition of the symmetry-independent part of the unit

TABLE I. Crystal data and structure refinement details for $URhGe_2$.

Parameter	Value
Compound	$URhGe_2$
M_I (g mol^{-1})	486.12
Crystal system, space group	Orthorombic, *Immm*
Temperature (K)	295
a, b, c (Å)	4.30056(11), 8.7463(2), 15.9570(3)
V(Å^3)	600.21(2)
Z	8
Radiation type	Mo $K\alpha$
μ (mm^{-1})	78.71
Crystal size (mm^3)	0.05×0.04×0.02
Diffractometer	Xcalibur, Atlas
Absorption coefficient	Gaussian
T_{min}, T_{max}	0.101, 0.281
No. of measured, independent, and observed [$I > 2\sigma(I)$] reflections	9142, 463, 443
R_{int}	0.053
$(\sin\theta/\lambda)_{max}$ (Å^{-1})	0.667
$R[F^2 > 2\sigma(F^2)]$, $wR(F^2)$, S	0.022, 0.048, 1.16
No. of reflections	463
No. of parameters	32
$\Delta\rho_{max}$, $\Delta\rho_{min}$ (e/Å^{-3})	6.08, −1.33

cell. It is worth noting that despite modeling the disorder, the U_{11} parameter for Ge1 remains four and three times larger than U_{22} and U_{33}, respectively. In addition, an elongated ellipsoid is also noticeable for Ge2. This effect is probably related to the layered structure of $URhGe_2$. Each layer consists of the atoms U2, Rh1, and Ge3. Neighboring layers are connected by the U1 atoms, and both Ge1 and Ge2 atoms are also located between the layers. The interlayer position of these two germanium atoms seems to be important for understanding the disorder and the large U_{11} parameter, especially why the germanium atoms are surrounded by the uranium and rhodium atoms with large ionic radius.

The thermodynamic properties of single-crystal $URhGe_2$ are summarized in Fig. 2. As shown in Fig. 2(a), the reciprocal magnetic susceptibility χ^{-1} in the paramagnetic region varies with temperature according to the modified Curie-Weiss law:

$$\chi = \left(\mu_{\text{eff}}^2/8\right)/(T-\theta_P) + \chi_0 \qquad (1)$$

TABLE II. Atomic coordinates and equivalent isotropic displacement parameters for $URhGe_2$. U_{eq} is defined as one third of the trace of the orthogonalized U_{ij} tensor.

Atom	x	y	z	U_{eq}
U(1)	0.5	0.23850(7)	0	0.01007(18)
U(2)	0.5	0	0.20634(3)	0.00611(18)
Rh(1)	0.5	0.24928(8)	0.35283(5)	0.0061(2)
Ge(1)	0.4545(18)	0	0.42363(12)	0.0136(15)
Ge(2)	0	0	0.07596(9)	0.0078(3)
Ge(3)	0.5	0.34652(12)	0.19670(6)	0.0071(2)

TABLE III. Anisotropic displacement parameters for the atoms in the $URhGe_2$ unit cell (in Å^2). For all atoms $U_{12} = 0$.

	U_{11}	U_{22}	U_{33}	U_{23}	U_{13}
U(1)	0.0070(3)	0.0157(3)	0.0076(3)	0	0
U(2)	0.0054(3)	0.0068(3)	0.0061(3)	0	0
Rh(1)	0.0058(4)	0.0059(4)	0.0065(4)	−0.0001(3)	0
Ge(1)	0.026(5)	0.0064(8)	0.0081(7)	0	0.0005(11)
Ge(2)	0.0111(7)	0.0068(7)	0.0054(6)	0	0
Ge(3)	0.0056(5)	0.0073(5)	0.0084(5)	−0.0017(4)	0

where μ_{eff}, θ_P, and χ_0 are the effective magnetic moment, the paramagnetic Curie-Weiss temperature, and the Pauli paramagnetic susceptibility, respectively. Least-squares fitting of this formula to the experimental data yields $\mu_{\text{eff}} = 2.9\mu_B$, $\theta_P = 20$ K, $\chi_0 = 4\times10^{-4}$ emu/mol. The thus derived effective magnetic moment is close to the value of $\mu_{\text{eff}} = 3.0\mu_B$

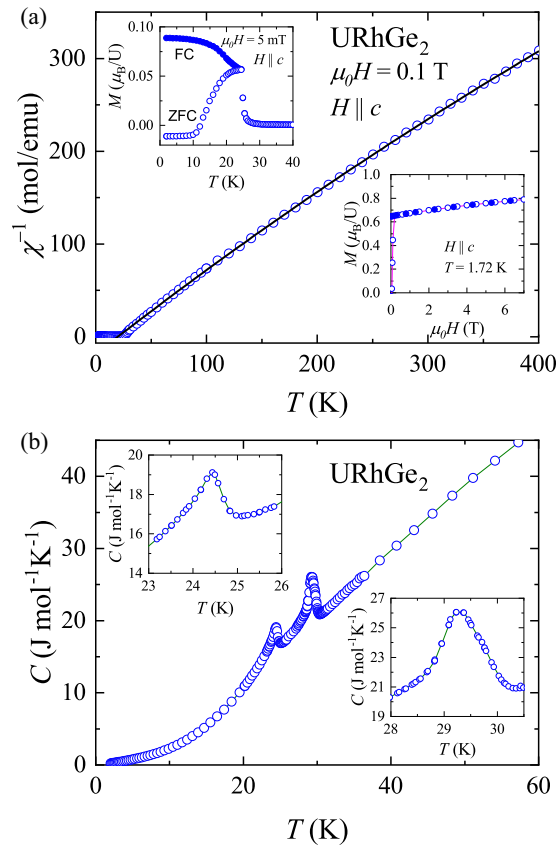

FIG. 2. (a) Inverse molar magnetic susceptibility of single-crystalline $URhGe_2$ as a function of temperature. The solid line represents the modified Curie-Weiss behavior. The top and bottom insets show the magnetization as a function of temperature and external magnetic field, respectively. The open and solid symbols in the top inset represent the data obtained in the zero-field-cooled and field-cooled modes, respectively. The open and solid symbols in the bottom inset represent the data obtained with increasing and decreasing magnetic field, respectively. The magnetic field was oriented along the crystallographic c direction. (b) Temperature dependence of the specific heat of $URhGe_2$. The insets show enlarged views of two peaks observed in the $C(T)$.

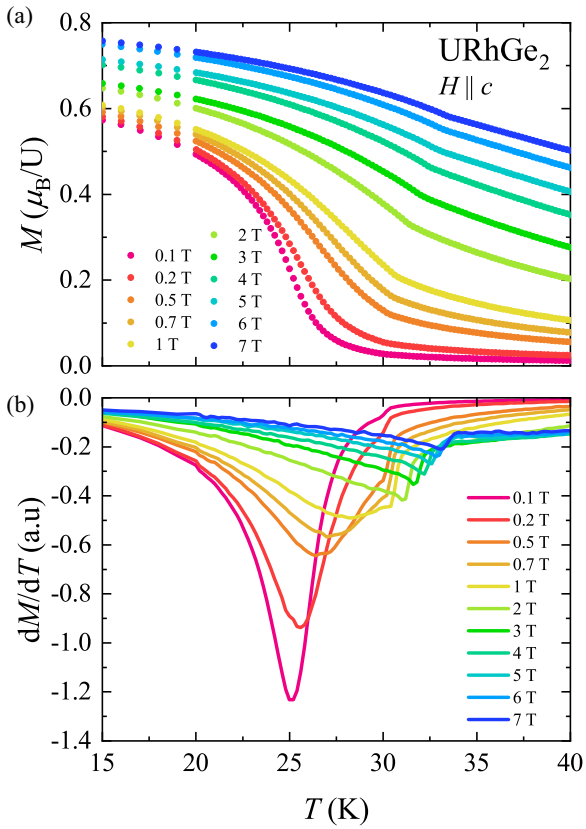

FIG. 3. (a) Magnetization of $URhGe_2$ measured between 15 and 40 K in selected magnetic fields in the range 0.1–7 T, oriented along the easy axis of magnetization. (b) First derivatives of the magnetization data.

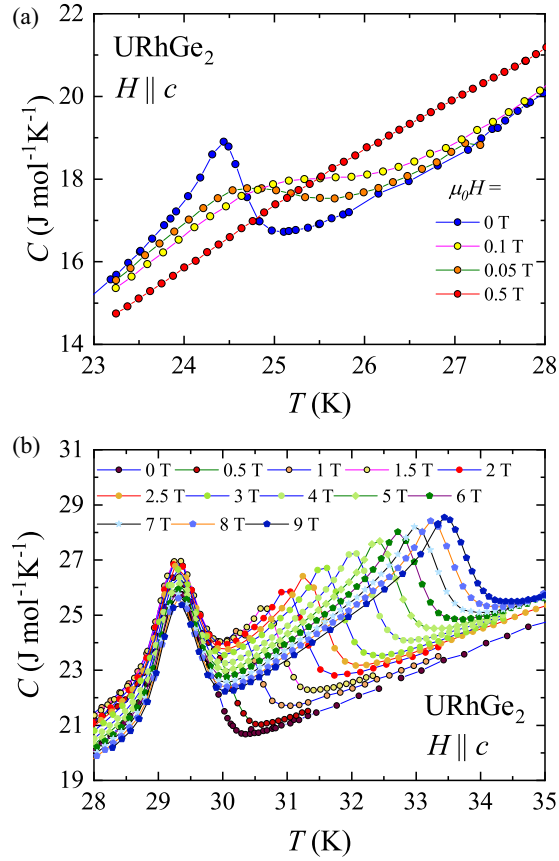

FIG. 4. The heat capacity of $URhGe_2$ measured at different magnetic fields in the range 0–9 T in the temperature interval (a) 23–28 K and (b) 28–35 K.

obtained in a previous study using the simple Curie-Weiss law [29]. This value is smaller than that predicted for free U^{3+} and U^{4+} ions ($3.62\mu_B$ and $3.58\mu_B$, respectively), most likely due to partial delocalization of U $5f$ electrons or crystal field effects. A positive value of θ_P indicates that the interactions between magnetic moments are mostly ferromagnetic.

As can be seen in the top inset in Fig. 2(a), at 25 K the magnetization as a function of temperature, measured in a small external field of 5 mT, changes in a steplike manner, which is characteristic of ferromagnets. Below 25 K the zero-field-cooled and field-cooled magnetizations are distinctly different, clearly demonstrating the presence of the ferromagnetic domains. However, as shown in the bottom inset in Fig. 2(a) a very small magnetic field of 0.05 T is required to reorient the magnetic moments within each domain along the direction of the external magnetic field. At higher magnetic fields the magnetization saturates, and the ordered moment measured at 7 T at a temperature of 1.72 K is $0.78\mu_B$, in agreement with the previously reported value [29].

The temperature variation of the heat capacity $C(T)$ of $URhGe_2$ below 60 K is shown in Fig. 2(b). As can be seen, there are two well-defined maxima in $C(T)$ which mark phase transitions and indicate the bulk nature of both. Their positions are in very good agreement with those previously reported, as well as with the estimated value of the electronic specific heat coefficient γ, which is 0.1 $\mathrm{J\,mol^{-1}\,K^{-2}}$ [29]. However, if we look more closely at the insets in Fig. 2(b), which cover the temperature range immediately around these peaks, we can see some tiny differences in their character. The peak observed at 25 K has a λ-like shape, while in the second case we can observe a slight broadening of the peak in the middle of its height.

B. H-T phase diagram

In order to shed more light on the possible origin of the anomaly in the $C(T)$ observed at 30 K we carried out detailed studies of the temperature dependence of the specific heat and magnetization in different external magnetic fields. The evolution of $M(T)$ with increasing magnetic field up to 7 T is shown in Fig. 3(a). At initial fields of 0.1 T there is still a well-defined jump in magnetization, although the transition is much broader than that observed at a field of 5 mT. With increasing magnetic field, the jump in $M(T)$ shifts towards higher temperatures, as expected for ferromagnets, while at higher fields, it becomes blurred, making it difficult to unambiguously define T_C above 1 T. At the same time, for a field of $B \simeq 1$ T, there is a very small kink in $M(T)$, which shifts slightly towards higher temperatures as the magnetic field increases. To study this anomaly in more detail, we determined the first derivatives of $M(T)$, shown in Fig. 3(b). The Curie temperature T_C, defined as the inflection point on the $M(T)$ curve, corresponds to the minimum in dM/dT. The

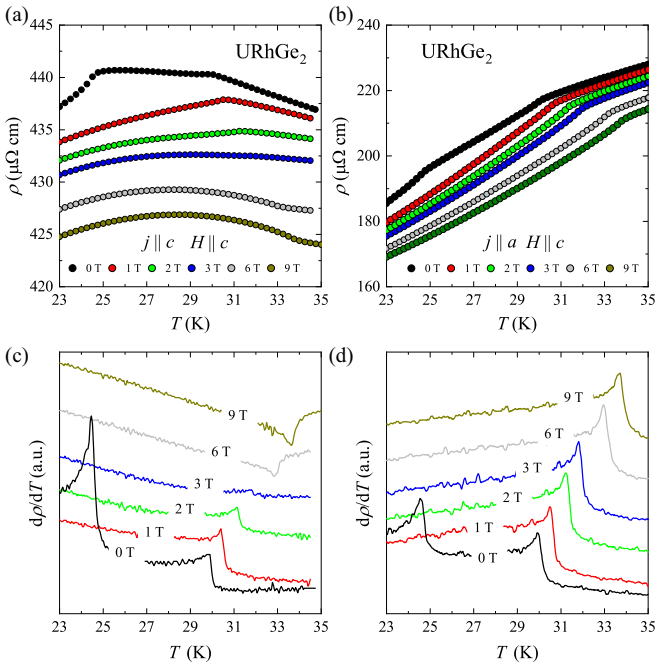

FIG. 5. (a) and (b) Zoom of the electrical resistivity anomalies measured along the crystallographic c axis and a axis, respectively. (c) and (d) First derivative of $\rho_c(T)$ and $\rho_a(T)$, respectively, showing the evolution of T_m with magnetic field.

so-derived Curie temperature is 25 K at 0.1 T, but as the field is increased, the minimum in dM/dT shifts towards higher temperatures, reaching 28.5 K at 1 T. Interestingly, a careful examination of dM/dT at $B < 1$ T reveals the presence of a small jump at $T_m = 30$ K, implying that the kink in $M(T)$ is, in fact, not induced by the magnetic field. The position of this anomaly overlaps with the onset of the jump in $C(T)$. This could also suggest that there is an additional phase transition near 30 K, but due to its small effect on the magnetization, it is hidden in the paramagnetic signal, just above T_C.

Figures 4(a) and 4(b) show the evolution of the maxima in $C(T)$ under an external magnetic field. As shown in Fig. 4(a), the magnetic field shifts the anomaly associated with T_C towards higher temperatures and reduces its magnitude. For a magnetic field of 0.5 T, only a barely visible hump in the temperature dependence of the heat capacity can be observed at about 26.5 K. Remarkably, the field evolution of the anomaly at 30 K is much more complex. At a field of 0.5 T the peak is initially broader, but at higher fields $B \geqslant 1$ T two subsequent maxima can be well distinguished on the $C(T)$ curves. Further increases in magnetic field show that the second peak shifts to higher temperatures, while the position of the first peak remains unaffected. This confirms our earlier suggestion that the broad anomaly observed at zero field is, in fact, composed of two closely spaced peaks.

The characteristic temperatures obtained from heat capacity and magnetization can be compared with those obtained from the resistivity measurements. The results of $\rho(T, B =$ const) for the two crystallographic directions, c and a, together with their first derivatives are shown in Fig. 5. The behavior is identical in both directions. In the absence of a magnetic field there are two anomalies whose positions

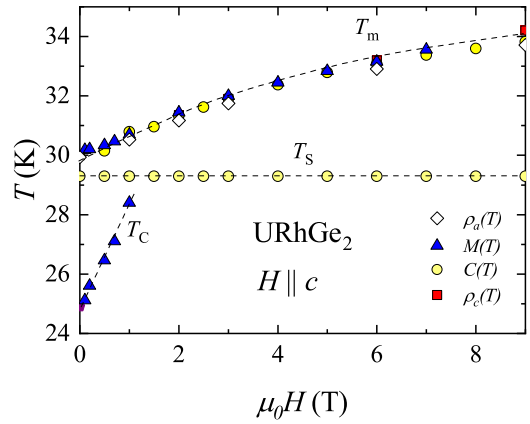

FIG. 6. Temperature-magnetic-field phase diagram of $URhGe_2$ determined for the magnetic field oriented along the easy axis of magnetization. The dashed lines are guides to the eyes.

coincide with T_C and T_m determined from magnetization and heat capacity. As the magnetic field strength increases, the anomaly at T_C vanishes for a field of 1 T. In turn, the evolution of T_m with field closely mirrors what is observed in the magnetic susceptibility. The kink in $\rho(T)$ shifts towards higher temperatures and reaches 34 K for a field of 9 T. It is noteworthy that, similar to the magnetization, the resistivity data show no anomaly at $T_s = 29.5$ K under applied magnetic fields. This suggests that structural changes in $URhGe_2$ are most likely minimal and have little effect on the conduction electron scattering. It is also worth noting that the residual resistivity in $URhGe_2$ is significant, being 10–30 times higher than in its nonmagnetic counterpart, $YPtGe_2$, depending on the crystallographic direction [27]. In this context, the detection of any changes in resistivity may prove challenging.

All the characteristic temperatures derived from the $C(T)$, $\sigma(T)$, and $\rho(T)$ curves are compiled in Fig. 6. On this constructed H-T phase diagram we can distinguish three lines representing phase transitions. The bottom line represents the transition to the ferromagnetic state. In the middle of the diagram there is a straight line formed by the phase transition points T_s. Remarkably, the transition temperature T_s remains constant at 29.5 K over the whole range of magnetic fields studied, indicating that $URhGe_2$ is likely to undergo a structural phase transition during cooling. This behavior mirrors that recently observed in isostructural compounds such as $YPtGe_2$ and $GdPtGe_2$ [27], in which structural transitions to the modulated phase occur below 174 and 145 K, respectively. It is concluded that these transitions are likely associated with increased U_{11} displacement parameters of the Ge1 atoms.

In the upper part of the diagram we observe an additional phase transition line, T_m. Although this characteristic temperature increases with the magnetic field, the observed anomaly in the heat capacity is not consistent with the behavior typically seen in ferromagnets. Furthermore, the response to the magnetic field does not match that of simple antiferromagnetic compounds, which typically show a decrease in T_N with increasing magnetic field strength. A similar behavior was recently observed in ferromagnetic URhSn with $T_C =$ 16 K [36]. The well-defined peak in $C(T)$ is accompanied by a small kink in the magnetic susceptibility at $T_0 = 54$ K. Similar

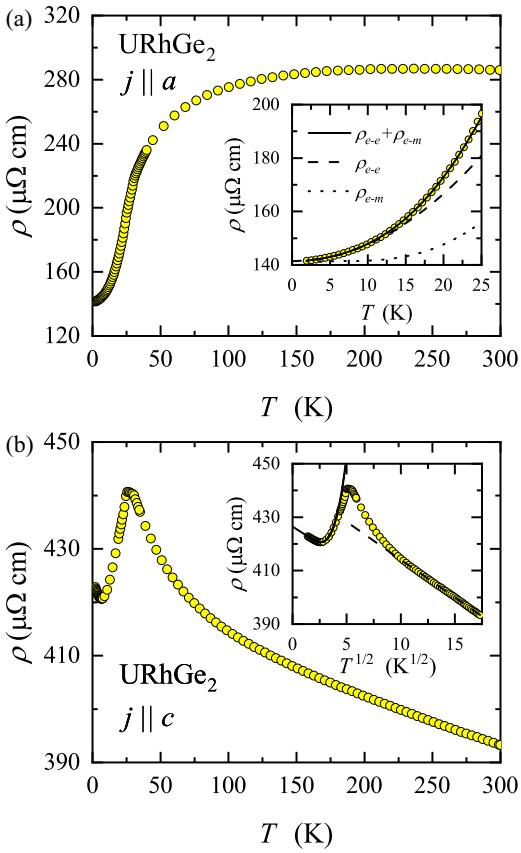

FIG. 7. (a) Resistivity of $URhGe_2$ measured along the crystallographic a axis. The inset shows the low-T region of ρ_a. The solid line represents the result of the least-squares fit of the experimental data for Eq. (2), while the dashed and dotted lines represent the Fermi liquid and electron spin wave scattering contributions, respectively. (b) Resistivity of $URhGe_2$ measured along the crystallographic a axis. The inset shows ρ_c versus $T^{1/2}$. The dashed and solid lines represent the fitting results using the $-T^{1/2}$ relation and modified Eq. (2), respectively (see text for a detailed description).

to the studied $URhGe_2$, this anomaly shifts slightly towards higher temperatures with increasing magnetic field. This behavior in the URhSn compound is thought to be related to a complex magnetic structure (e.g., canted antiferromagnetic or helimagnetic ordering) or to the presence of quadrupole ordering. However, since we do not observe any effect of the magnetic field on the height of the peak in $C(T)$, it is more likely that the transition at T_m in the studied $URhGe_2$ is associated with multipole ordering. Interestingly, in some cases of antiferroquadrupolar phases, the ordering temperature also shifts to higher values with increasing magnetic field strength [37].

C. The interplay between ferromagnetic order and atomic disorder

Figures 7(a) and 7(b) show the resistivities of $URhGe_2$ measured along the crystallographic a axis (ρ_a) and c axis (ρ_c) in the temperature range 2–300 K. At higher temperatures the resistivity ρ_a is almost temperature independent. This suggests that the electron-phonon interaction is less important in this case and that the dominant scattering mechanism in the paramagnetic regime is spin disorder scattering. Below about 150 K ρ_a decreases down to the lowest temperature of the experiment. $\rho_a(T)$ in the ferromagnetic range can be fitted with the expression

$$\rho(T) = \rho_0 + A_{\mathrm{FL}}T^2 + a\Delta T \exp\left(-\frac{\Delta}{T}\right)\left(1 + \frac{2T}{\Delta}\right), \quad (2)$$

where the first term represents the residual resistivity, the second term is a Fermi liquid term, and the third term represents a contribution due to electron-magnon scattering [38]. A_{FL} and a are proportional coefficients, while Δ denotes the energy gap in the magnon spectrum. As shown by the solid line in the inset of Fig. 7(a), the experimental data are very well reproduced by the above expression with $\rho_0 = 141\ \mu\Omega\,\mathrm{cm}$, $a = 0.045\ \mu\Omega\,\mathrm{cm\,K^{-2}}$, $\Delta = 51.5$ K, and $A_{\mathrm{FL}} = 0.063\ \mu\Omega\,\mathrm{cm\,K^{-2}}$. Comparing the individual components of the temperature dependence of the resistivity, it can be seen that the low-temperature region is dominated by the Fermi liquid contribution, which is consistent with the rather large γ value observed in the specific heat. Furthermore, due to the large value of Δ, electron scattering from the spin waves is ineffective when $T \ll \Delta$.

In contrast, the temperature variation of ρ_c is very different from ρ_a. Throughout the paramagnetic range, the resistivity ρ_c increases with decreasing temperature. Initially, between room temperature and about 100 K, the resistivity follows the $T^{1/2}$ dependence. Below 100 K, however, the increase in resistivity becomes more pronounced up to a temperature of 30 K. At 30 K there is a sharp anomaly in $\rho_c(T)$, below which the resistivity continues to increase, reaching its maximum value at 25 K. Below T_{C} the resistivity decreases due to the reduction in the spin disorder resistivity, but remarkably, it does not asymptotically approach the constant value as one would expect for typical ferromagnetic compounds. The decrease in resistivity is interrupted by the local minimum at a temperature of 7 K, below which the resistivity again changes as $T^{1/2}$, in a manner analogous to that observed in the paramagnetic state for $T \gg T_{\mathrm{C}}$.

It is also worth noting that the residual resistivity ratio $\rho(300\ \mathrm{K})/\rho(2\ \mathrm{K})$ is only 0.93, which is two times lower than the corresponding value obtained for the crystallographic c axis. The near-unity value of this ratio, together with a large residual resistivity, which is as high as 440 $\mu\Omega\,\mathrm{cm}$, indicates that the conductivity along this direction is strongly limited by electron scattering off imperfections in the crystal structure. The origin of the minimum in $\rho_c(T)$ can therefore be explained as a result of the competition between classical and quantum phenomena in diffusive electron transport, which are responsible for positive and negative contributions to the temperature coefficient of resistivity (TCR), respectively.

Consequently, assuming that below T_{C} the classical transport is mainly governed by electron-spin wave scattering, $\rho_c(T)$ in the ferromagnetic state can be approximated by relation (2), but with the Fermi liquid term replaced by the electron interaction quantum correction $A_{\mathrm{QC}}T^{1/2}$ (also known as the Altshuler-Aronov quantum correction) [39,40]. The best fit between 2 and 20 K gives $\rho_0 = 426\ \mu\Omega\,\mathrm{cm}$, $a = 0.045\ \mu\Omega\,\mathrm{cm\,K^{-2}}$, $\Delta = 15$ K, and $A_{\mathrm{QC}} = -2.61\ \mu\Omega\,\mathrm{cm\,K^{-1/2}}$. These results indicate that a is

comparable to that obtained for the a axis, while the gap of the ferromagnetic spin waves is anisotropic over the two examined current directions. In turn, the A_{QC} coefficient has rather moderate values. For example, in La_2NiSi_3, which can be classified as a weakly disordered compound, the increase in $\rho(T)$ is relatively small, giving $A_{QC} = -0.053\ \mu\Omega\,\mathrm{cm\,K}^{-1/2}$ [41]. On the other hand, it can reach very high values in the case of highly disordered compounds. Recently, it was that in the half-Heusler YPdSb $A_{QC} = -170\ \mu\Omega\,\mathrm{cm\,K}^{-1/2}$, which causes the $T^{1/2}$ dependence of the resistivity to extend to temperatures as high as 80 K [42].

It is worth noting that quantum corrections have also been well documented in disordered ferromagnets and spin glasses in various studies [43–48]. However, among single-crystalline compounds, $URhGe_2$ stands out for its unique property of exhibiting the absence of quantum corrections in resistivity along a specific crystallographic direction, namely, the a axis. In general, the magnitude of the interaction quantum corrections is typically quantified by the coefficient A_{QC}, which is mainly influenced by the residual resistivity. Another crucial aspect to consider is how the resistivity associated with classical electron transport evolves with temperature above the minimum. Since $\rho_c/\rho_a \approx 3$ and ρ_a experiences a rapid decline below T_C due to the damping of spin wave excitations, the minimum does not appear in $\rho_a(T)$.

Similar to low-temperature resistivity, the absence of a negative TCR in ρ_a can be attributed to the much longer mean free path associated with atomic and spin disorder scattering along the crystallographic a axis compared to the c axis. Furthermore, there may be an additional mechanism relevant to disordered ferromagnets which takes into account the interplay between weak localization and critical spin fluctuations when the mean free path is shorter than the magnetic correlation length [49]. In this context it has been shown that the temperature-dependent resistivity as one approaches T_C from above depends on the strength of the spin-orbit coupling. When the spin-orbit coupling is robust, the resistivity exhibits a more pronounced anomaly due to conduction electron scattering from spin fluctuations than would be predicted by classical approaches based on Boltzmann theory. Conversely, in the absence of significant spin-orbit coupling, the opposite scenario is observed; namely, the resistivity decreases with decreasing temperature when the magnetic correlation length becomes comparable to the mean free path. These two extreme cases may provide insight into the temperature dependence of ρ_a and ρ_c in the studied $URhGe_2$ under the assumption of weak and strong spin-orbit coupling in these two crystallographic directions, respectively.

It is important to note that when studying the transport properties of f-electron systems in the paramagnetic regime, they are typically approached from the perspective of the Kondo effect, regardless of the strength of impurity scattering. However, as shown in Fig. 7(b), the resistivity ρ_c at temperatures well above the critical temperature ($T \gg T_C$) does not exhibit the characteristic logarithmic dependence on temperature associated with the Kondo effect and instead follows a $T^{1/2}$ relationship. Interestingly, if we fit the $A_{QC}T^{1/2}$ relationship to the resistivity data in the temperature range of 100 to 300 K, we obtain a value of $A_{QC} = -2.83\ \mu\Omega\,\mathrm{cm\,K}^{-1/2}$,

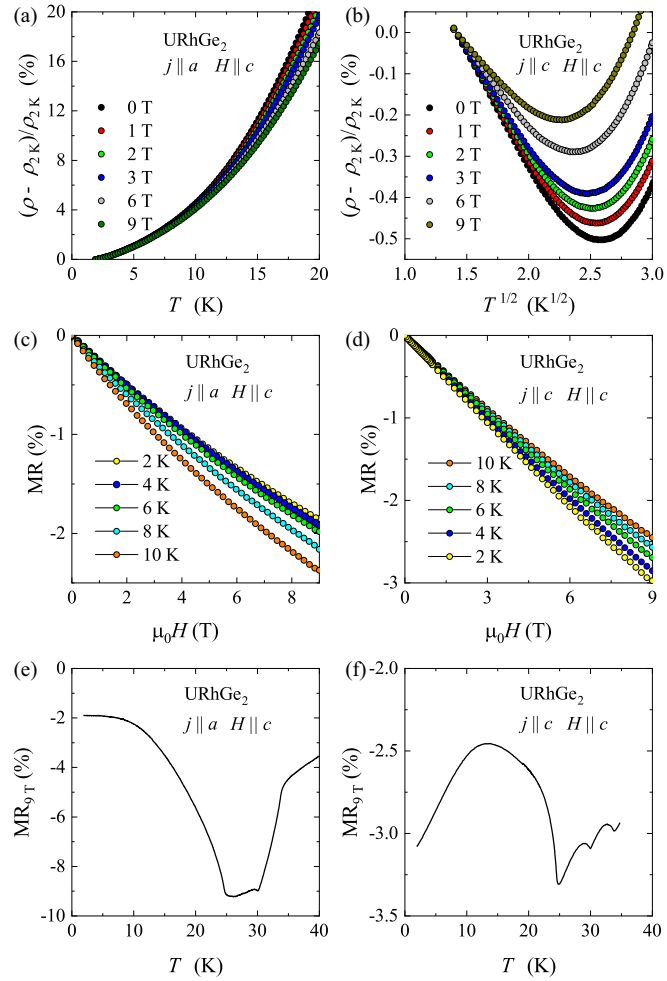

FIG. 8. (a) and (b) The resistivities ρ_a and ρ_c of $URhGe_2$ measured at low temperatures in selected magnetic fields in the range 0–9 T. (c) and (d) The magnetoresistances MR_a and MR_c versus external magnetic field at 2, 4, 6, 8, and 10 K. (e) and (f) The magnetoresistances MR_a and MR_c as a function of temperature, measured for a magnetic field of 9 T.

which closely matches the value derived from the analysis at lower temperatures. The slight increase in the coefficient A_{QC} for $T \gg T_C$ can be attributed to the shorter mean free path, as the conduction electrons experience increased scattering due to both spin disorder and atomic disorder in the paramagnetic state.

It is also worth noting that there are alternative mechanisms related to enhanced electron disorder scattering that can explain the negative TCR. One such mechanism is an extension of the Faber-Ziman theory [50], while the other is associated with disorder-assisted polaron formation [51]. It is important to note that these mechanisms do not exclude the presence of quantum corrections; however, they lead to a resistivity that follows a linear or quasilinear dependence on temperature at higher temperature limits, which is significantly different from the behavior observed in the studied $URhGe_2$.

The influence of a magnetic field on the resistivities ρ_a and ρ_c in the ferromagnetic state is shown in Figs. 8(a) and 8(b), respectively. In particular, $\rho_a(T)$ remains unchanged by the

external magnetic field below 6 K, whereas the increase in $\rho_c(T)$ is attenuated with increasing field strength, leading to a slight shift of the minimum in $\rho_a(T)$ towards lower temperatures. This behavior is different from what would be expected for nonmagnetic disordered conductors, in which interaction corrections are typically weakly affected by magnetic fields. This suggests the possibility of additional corrections contributing to the increase in resistivity at low temperatures. This hypothesis is supported by the results of magnetoresistance (MR) measurements made as a function of both magnetic field and temperature, shown in Figs. 8(c) and 8(d) and 8(e) and 8(f), respectively. Although both $|\mathrm{MR_a}|$ and $|\mathrm{MR_c}|$ are negative and vary with field in a similar way, their temperature dependences are different. In particular, $|\mathrm{MR_a}|$ increases with increasing temperature and reaches its maximum at the critical temperature T_C, as expected for ferromagnetic materials [52,53]. On the other hand, the magnitude of $|\mathrm{MR_c}|$ shows a nonmonotonic behavior. Unlike $|\mathrm{MR_a}|$, which converges to a constant value, $|\mathrm{MR_c}|$ increases below 14 K. This observation implies that while the primary contribution to the negative magnetoresistance in both crystallographic directions is due to the suppression of spin fluctuation excitations, there is an additional negative contribution to $|\mathrm{MR_c}|$ responsible for the reduction of the low-temperature rise of $\rho_c(T)$ in the presence of an external magnetic field. This additional quantum correction being susceptible to magnetic field can be attributed to the weak localization effect, which can induce negative magnetoresistance in the presence of spin-orbit interactions in ferromagnetic systems [54,55]. Furthermore, the presence of another quantum correction to the conductivity, such as the spin wave mediated Altshuler-Aronov correction [56–58], cannot be ruled out. It is important to note that this type of correction is specific to magnetically ordered systems and has been identified in only a limited number of compounds [58–60].

IV. SUMMARY

We carried out a comprehensive investigation of the physical properties of the locally noncentrosymmetric ferromagnet $URhGe_2$ using single-crystalline samples. Our results revealed an additional singularity in the specific heat within the paramagnetic region, in close proximity to the previously discovered phase transition at 30 K. The slight variations in the characteristic temperatures of these phase transitions cause them to overlap, forming a broad peak below 30 K. Interestingly, our analysis showed that these transitions respond differently to an external magnetic field, implying different natures for each. By studying the influence of the magnetic field on the characteristic temperatures, we constructed a phase diagram. This diagram shows that one of these transitions is independent of the external magnetic field, indicating that it could be considered a structural phase transition. In contrast, the characteristic temperature of the other phase transition shifts to higher temperatures with increasing magnetic field. The nature of these changes is complicated and does not fit either antiferromagnetic or ferromagnetic transitions. We hypothesize that it may be related to multipole ordering, but further investigation is essential to clarify the nature of these two phase transitions and their possible interrelationships.

In addition, our research highlights the relationship between the temperature dependence of the resistivity of single-crystalline $URhGe_2$ along the a and c crystallographic axes and the magnitude of the residual resistivity. A lower residual resistivity ρ_a compared to ρ_c suggests that electron transport in the a direction can be treated classically. However, since ρ_c is three times higher than ρ_a, the influence of disorder on electron transport in the c direction cannot be ignored. Consequently, the low-temperature resistivity ρ_a is dominated by the $A_{\mathrm{FL}}T^2$ contribution, which is characteristic of the electron-electron interaction in a clean system. Meanwhile, the electron-electron interaction in the presence of significant impurity scattering causes the Altshuler-Aronov correction $A_{\mathrm{QC}}T^{1/2}$ to become essential in the temperature dependence of ρ_c. In the ferromagnetic state, this interaction correction competes with electron spin wave scattering, leading to a minimum in the $\rho_c(T)$, similar to transition-element-deficient $UT_{1-x}Ge_2$ compounds. Notably, our results show that the interaction correction remains relevant in the paramagnetic state, likely due to the spin disorder resistivity contribution. At $T > T_C$ this additional scattering mechanism adds to the scattering of conduction electrons on atomic disorder, leading to a reduction of the mean free path, thus creating the possibility to observe a quantum correction above T_C.

[1] M. H. Fischer, M. Sigrist, D. F. Agterberg, and Y. Yanase, Annu. Rev. Condens. Matter Phys. **14**, 153 (2023).

[2] D. Maruyama, M. Sigrist, and Y. Yanase, J. Phys. Soc. Jpn. **81**, 034702 (2012).

[3] T. Watanabe, T. Yoshida, and Y. Yanase, Phys. Rev. B **92**, 174502 (2015).

[4] F. Piccinelli, I. Carrasco, C.-G. Ma, A. M. Srivastava, and M. Bettinelli, Inorg. Chem. **57**, 9241 (2018).

[5] R. Streubel, D. S. Bouma, F. Bruni, X. Chen, P. Ercius, J. Ciston, A. T. N'Diaye, S. Roy, S. D. Kevan, P. Fischer, and F. Hellman, Adv. Mater. **33**, 2004830 (2021).

[6] R. Milkus and A. Zaccone, Phys. Rev. B **93**, 094204 (2016).

[7] A. Ashoka, S. Nagane, N. Strkalj, A. Sharma, B. Roose, A. J. Sneyd, J. Sung, J. L. MacManus-Driscoll, S. D. Stranks, S. Feldmann, and A. Rao, Nat. Mater. **22**, 977 (2023).

[8] M. H. Fischer, F. Loder, and M. Sigrist, Phys. Rev. B **84**, 184533 (2011).

[9] J. Goryo, M. H. Fischer, and M. Sigrist, Phys. Rev. B **86**, 100507(R) (2012).

[10] M. Sigrist, D. F. Agterberg, M. H. Fischer, J. Goryo, F. Loder, S.-H. Rhim, D. Maruyama, Y. Yanase, T. Yoshida, and S. J. Youn, J. Phys. Soc. Jpn. **83**, 061014 (2014).

[11] S. Khim, J. F. Landaeta, J. Banda, N. Bannor, M. Brando, P. M. R. Brydon, D. Hafner, R. Küchler, R. Cardoso-Gil, U. Stockert, A. P. Mackenzie, D. F. Agterberg, C. Geibel, and E. Hassinger, Science **373**, 1012 (2021).

[12] S. Hayami, H. Kusunose, and Y. Motome, J. Phys. Soc. Jpn. **84**, 064717 (2015).

[13] Y. Yanase, J. Phys. Soc. Jpn. **83**, 014703 (2014).

[14] L. Fu, Phys. Rev. Lett. **115**, 026401 (2015).

[15] E. van Walsem, R. A. Duine, and M. H. D. Guimarães, Phys. Rev. B **102**, 174403 (2020).

[16] J.-Z. Fang, S. Wang, X.-G. Ye, B.-C. Lin, A.-Q. Wang, H.-N. Cui, J.-K. Wang, G.-Y. Zhu, S. Liu, Y. Li, Z. Wang, Y. Yao, Z. Wei, D. Yu, and Z.-M. Liao, Phys. Rev. B **104**, 054409 (2021).

[17] S. S. Saxena, P. Agarwal, K. Ahilan, F. M. Grosche, R. K. W. Haselwimmer, M. J. Steiner, E. Pugh, I. R. Walker, S. R. Julian, P. Monthoux, G. G. Lonzarich, A. Huxley, I. Sheikin, D. Braithwaite, and J. Flouquet, Nature (London) **406**, 587 (2000).

[18] D. Aoki, A. Huxley, E. Ressouche, D. Braithwaite, J. Flouquet, J. P. Brison, E. Lhotel, and C. Paulsen, Nature (London) **413**, 613 (2001).

[19] N. T. Huy, A. Gasparini, D. E. de Nijs, Y. Huang, J. C. P. Klaasse, T. Gortenmulder, A. de Visser, A. Hamann, T. Görlach, and H. v. Löhneysen, Phys. Rev. Lett. **99**, 067006 (2007).

[20] D. Aoki and J. Flouquet, J. Phys. Soc. Jpn. **83**, 061011 (2014).

[21] M. Szlawska, M. Pasturel, D. Kaczorowski, and A. Pikul, J. Alloys Compd. **892**, 162032 (2022).

[22] M. Pasturel, M. Szlawska, J. Ćwik, D. Kaczorowski, and A. Pikul, Intermetallics **131**, 107112 (2021).

[23] A. P. Pikul, M. Szlawska, X. Ding, J. Sznajd, M. Ohashi, D. A. Kowalska, M. Pasturel, and K. Gofryk, Phys. Rev. Mater. **6**, 104408 (2022).

[24] M. Pasturel, A. Pikul, G. Chajewski, H. Noëla, and D. Kaczorowski, Intermetallics **95**, 19 (2018).

[25] M. Henriques, D. Berthebaud, A. Lignie, Z. El Sayah, C. Moussa, O. Tougait, L. Havela, and A. Gonçalves, J. Alloys Compd. **639**, 224 (2015).

[26] G. Guy, M. Szlawska, C. Prestipino, V. Dorcet, V. Demange, P. Fertey, D. Kaczorowski, M. Pasturel, and A. Pikul, J. Solid State Chem. **319**, 123795 (2023).

[27] O. Janka, R.-D. Hoffmann, B. Heying, and R. Pöttgen, Dalton Trans. **47**, 6075 (2018).

[28] E. Hickey, B. Chevalier, and J. Etourneau, Mater. Res. Bull. **24**, 1111 (1989).

[29] T. D. Matsuda, Y. Haga, Y. Tokiwa, G. Andrei, and E. Yamamoto, Acta Phys. Pol. B **34**, 1071 (2003).

[30] T. D. Matsuda, S. Ikeda, Y. Haga, E. Yamamoto, M. Hedo, Y. Uwatoko, and Y. Onuki, J. Phys.: Condens. Matter **15**, S2019 (2003).

[31] G. M. Sheldrick, Acta Cryst. A **71**, 3 (2015).

[32] G. M. Sheldrick, Acta Cryst. **C71**, 3 (2015).

[33] C. B. Hübschle, G. M. Sheldrick, and D. Birger, J. Appl. Cryst. **44**, 1281 (2011).

[34] K. Brandenburg and H. Putz, Diamond: Crystal and Molecular Structure Visualization (2008).

[35] The Materials Project, 2019.

[36] Y. Shimizu, A. Miyake, A. Maurya, F. Honda, A. Nakamura, Y. J. Sato, D. Li, Y. Homma, M. Yokoyama, Y. Tokunaga, M. Tokunaga, and D. Aoki, Phys. Rev. B **102**, 134411 (2020).

[37] T. Sakakibara, T. Tayama, K. Tenya, M. Yokoyama, H. Amitsuka, D. Aoki, Y. Ōnuki, Z. Kletowski, and S. Kunii, J. Phys. Chem. Solids **63**, 1147 (2002).

[38] M. B. Fontes, J. C. Trochez, B. Giordanengo, S. L. Bud'ko, D. R. Sanchez, E. M. Baggio-Saitovitch, and M. A. Continentino, Phys. Rev. B **60**, 6781 (1999).

[39] B. L. Altshuler and A. G. Aronov, Zh. Eksp. Teor. Fiz. **77**, 2028 (1979) [Sov. Phys. JETP **50**, 968 (1979)].

[40] B. L. Altshuler and A. G. Aronov, *Electron-Electron Interactions in Disordered Systems* (Elsevier, Amsterdam, 1985).

[41] D. Gnida, M. Szlawska, P. Swatek, and D. Kaczorowski, J. Phys.: Condens. Matter **28**, 435602 (2016).

[42] D. Gnida, K. Ciesielski, and D. Kaczorowski, Phys. Rev. B **103**, 174206 (2021).

[43] C. P. Moca, B. L. Sheu, N. Samarth, P. Schiffer, B. Janko, and G. Zarand, Phys. Rev. Lett. **102**, 137203 (2009).

[44] L. Havela, M. Paukov, V. Buturlim, I. Tkach, D. Drozdenko, M. Cieslar, S. Mašková, M. Dopita, and Z. Matěj, Phys. Rev. B **95**, 235112 (2017).

[45] A. Otop, S. Süllow, M. B. Maple, A. Weber, E. W. Scheidt, T. J. Gortenmulder, and J. A. Mydosh, Phys. Rev. B **72**, 024457 (2005).

[46] S. Süllow, I. Maksimov, A. Otop, F. J. Litterst, A. Perucchi, L. Degiorgi, and J. A. Mydosh, Phys. Rev. Lett. **93**, 266602 (2004).

[47] D. Gnida, M. Szlawska, P. Wiśniewski, and D. Kaczorowski, Acta Phys. Pol. A **127**, 451 (2015).

[48] M. Szlawska, D. Kaczorowski, and M. Reehuis, Phys. Rev. B **81**, 094423 (2010).

[49] C. Timm, M. E. Raikh, and F. von Oppen, Phys. Rev. Lett. **94**, 036602 (2005).

[50] P. J. Cote and L. V. Meisel, Phys. Rev. Lett. **40**, 1586 (1978).

[51] S. Ciuchi, D. D. Sante, V. Dobrosavljević, and S. Fratini, npj Quantum Mater. **3**, 44 (2018).

[52] H. Yamada and S. Takada, Prog. Theor. Phys. **48**, 1828 (1972).

[53] S. N. Kaul, J. Phys.: Condens. Matter **17**, 5595 (2005).

[54] V. K. Dugaev, P. Bruno, and J. Barnaś, Phys. Rev. B **64**, 144423 (2001).

[55] V. K. Dugaev, P. Bruno, and J. Barnaś, Phys. Rev. Lett. **101**, 129701 (2008).

[56] J. Danon, A. Ricottone, and P. W. Brouwer, Phys. Rev. B **90**, 024405 (2014).

[57] K. A. Muttalib and P. Wölfle, Phys. Rev. B **91**, 144410 (2015).

[58] R. Misra, A. F. Hebard, K. A. Muttalib, and P. Wölfle, Phys. Rev. B **79**, 140408(R) (2009).

[59] S. Buvaev, S. Ghosh, K. Muttalib, P. Wölfle, and A. Hebard, Phys. Rev. B **90**, 214429 (2014).

[60] M. Szlawska, D. Gnida, P. Ruszała, M. J. Winiarski, M. Samsel-Czekała, M. Schmidt, Y. Grin, and D. Kaczorowski, Materials **13**, 3865 (2020).